The International Journal of Advanced Manufacturing Technology
https://doi.org/10.1007/s00170-025-15329-w

ORIGINAL ARTICLE

Autonomous direct freeform fabrication strategy for multi-axis additive manufacturing

Xinyi Xiao[1] · Yousub Lee[2] · Thomas Feldhausen[2,3]

Received: 11 November 2024 / Accepted: 26 February 2025

Abstract
Multi-axis additive manufacturing (M-AM) enables precise material deposition along both planar and curved layers, eliminating the need for support structures through a continuous material deposition approach. In contrast to conventional 2-dimensional planar layers constrained to a fixed building orientation, the deposition on freeform layers demands the specification of *guided curves* to determine material deposition directions which are no longer to be fixed to a build direction. There are challenges that arise when fabricating components with multiple "build" directions, necessitating the decomposition of geometries and the specification of guided curves for the resulting volumes. Furthermore, multi-axis systems introduce heightened challenges due to an increased degree of freedom in motion. Consequently, the potential risks of collision between the deposited geometry and the motion platform become a notable concern. This research proposes a freeform layering algorithm to address the challenge of seamless transitions between planar and curved layers in the process planning of M-AM. The algorithm computes 3D "printable" layers by leveraging topological information derived from the geometry to be built and integrates collision-free manufacturability considerations into the computational process. These accumulated volumes serve as a "substrate" and support volumes for subsequent deposition, allowing later layers to be built without the need for additional support material. The proposed method successfully devises a freeform layering approach suitable for intricate models that demand substantial support, thus enabling the fabrication of diverse geometries in a manner previously unachievable.

Keywords Multi-axis AM · 3D "printable" layers · Collision-free · Freeform

1 Introduction

Traditional layer by layer additive manufacturing (AM) methodologies, originating in the 1980s, have undergone continuous refinement. These techniques enable the fabrication of parts with heightened geometric complexity by employing a deposition process along a build direction, necessitating support structures beneath overhanging surfaces. Given the varying support requirements for different build orientations, substantial research efforts have been dedicated to optimizing build orientations with the aim of minimizing the requisite support material [1–3]. Computer-based simulations have proven instrumental in generating optimized results based on user inputs. However, the process of support structure removal, particularly challenging for metal parts, has not been comprehensively addressed in existing optimization approaches. Consequently, there is a growing emphasis on the development of process planning methodologies for multi-axis AM that enable the construction of parts without relying on support structures [4–6],

✉ Xinyi Xiao
Xinyi.Xiao@unt.edu

[1] Department of Mechanical Engineering, University of North Texas, Denton, TX, USA

[2] Manufacturing Demonstration Facility, Oak Ridge National Laboratory, Oak Ridge, TN, USA

[3] Aerospace and Mechanical Engineering, University of Texas at El Paso, El Paso, TX, USA

Published online: 14 March 2025

while ensuring the success of the print. In this context, 5-axis AM [7], characterized by a robotic system with a two additional rotary table, compared to traditional 3-axis AM, presents a promising solution to the challenges associated with support structures. This advanced process is often referred to as multi-axis support-free additive manufacturing, or M-AM system [8].

In current industrial software implementations for M-AM, the user is typically responsible for manually decomposing a complex part into discrete additive volumes, often referred to as sub-volumes or build regions, to accommodate available tool-path strategies within the software's library. This decomposition process is a critical step in ensuring manufacturability, as each sub-volume must be assigned a suitable tool path strategy that aligns with the machine's capabilities and constraints. Once the part is decomposed, these sub-volumes are mapped to predefined tool path strategies, which may include raster-based deposition, contour-based toolpaths, spiral or helical toolpaths, or hybrid approaches. The selection of the appropriate strategy is influenced by several factors, including the geometry of the sub-volume, the layer deposition sequence, and the desired surface quality. However, in cases where no direct mapping exists between a decomposed volume and the available tool-path strategies, further refinement of the decomposition is required. This could involve introducing additional partitions or adopting novel decomposition techniques such as feature-based segmentation, geometric heuristics, or topology-based partitioning to ensure compatibility with the additive process. The current multi-axis deposition approaches can be categorized into following:

- *Multi-volume decomposition approach* (Fig. 1a): Fig. 1 a depicts the multi-volume decomposition approach [4–6], where the part is decomposed into multiple volumes, each independently processed without the need for support structures. While this method offers a more straightforward and intuitive solution, it may require intricate decomposition strategies to accommodate complex geometries, potentially leading to increased manual intervention in the decomposition process.
- *Adaptive slicing approach* (Fig. 1b): In this approach, the generation of support-free toolpaths is achieved through adaptive slicing [7–9], wherein the layer thickness is dynamically adjusted based on the local geometry of the part. This method is advantageous in mitigating the need for explicit support structures by adaptively altering the deposition thickness. However, it may introduce challenges in maintaining uniform build quality across the entire part due to variations in layer thickness resulting in non-uniform heat input.
- *Conformal sweeping approach* (Fig. 1c): It involves the systematic traversal of the deposition toolhead along the contours of the target surface, ensuring a seamless and conformal layering [10] of material. This approach is characterized by its adaptability to intricate geometries and the ability to address challenges posed by varying surface curvatures.

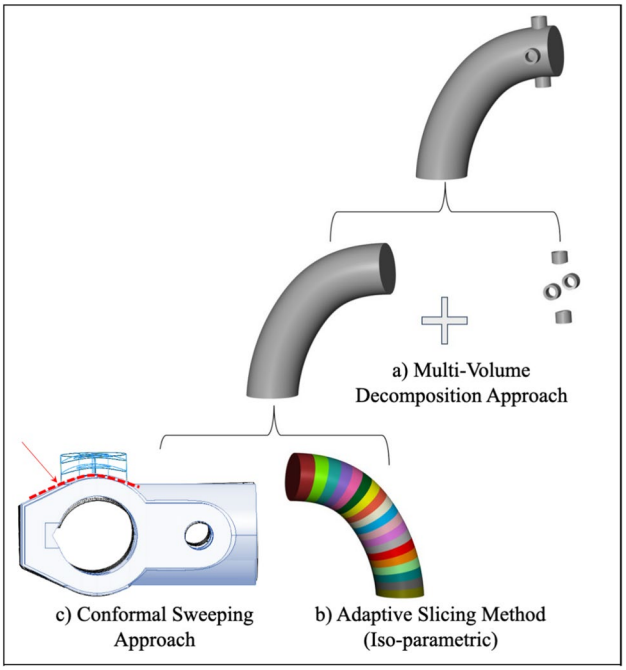

Fig. 1 Current M-AM manufacturing strategies

Within the realm of the M-AM system, the formulation of a robust freeform fabrication strategy necessitates careful consideration of two distinct types of collisions—local and global—which are integral to ensuring a feasible and efficient deposition process (as visualized in Fig. 2). Failure to address these collisions can result in defects, tool crashes, or even complete process failures, thereby compromising both the accuracy and integrity of the manufactured part. These collisions are categorized as follows:

- *Local collision*—tool and as-deposited part: defined by interactions between the deposition head and the sections of the part that have already been fabricated.
- *Global collision*—tool, substrate, fixture, and machine: involves potential collisions between the deposition tool, motion system, and every system components, including setup.

Addressing both local and global collisions is imperative in formulating a comprehensive and fail-safe freeform fabrication strategy within the M-AM system. More specifically, toolpath execution in M-AM requires continuous reorientations to maintain optimal deposition angles, but excessive

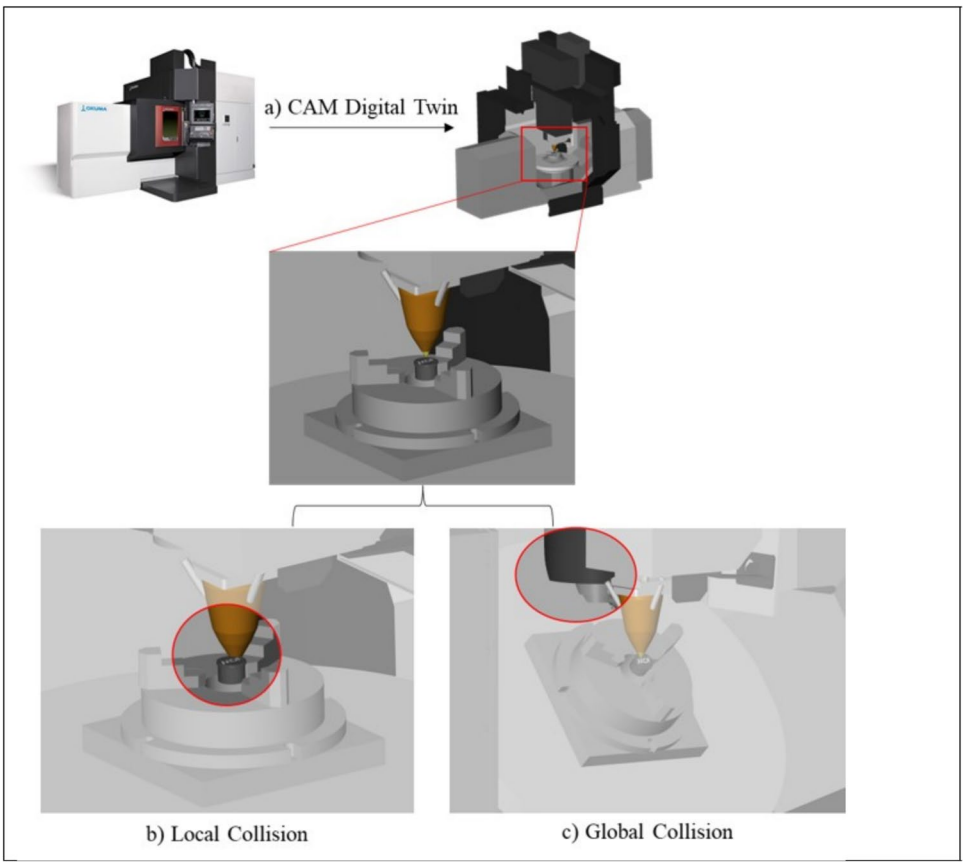

Fig. 2 Potential collision on M-AM system **a** CAM view of the M-AM system, **b** local collision, and **c** global collision

tilts may lead to collisions between the tool head and machine structures or violate kinematic constraints, such as exceeding axis travel limits. Certain robotic and CNC-based 5-axis systems encounter kinematic singularities, where specific joint configurations result in undefined motion behavior, causing abrupt stops or excessive joint torque demands. To ensure smooth and stable transitions, path planning algorithms must account for these constraints by optimizing motion sequences and avoiding problematic configurations. Additionally, tool repositioning moves—such as retracting the nozzle to a safe position before reapproaching another region—can introduce unintended collisions if not properly planned. Computing safe tool retraction paths is essential to minimize travel time while maintaining adequate clearance and avoiding interference with the deposited structure or machine components.

Model decomposition has recently been widely used in the context of MAM fabrication. This integration aims to optimize material utilization and alleviate challenges associated with the post-fabrication removal of support structures. Existing multi-axis deposition strategies based on decomposition, as presented in Zhang [7] and Luo [9], predominantly adhere to a 2D layer deposition paradigm when fabricating each decomposed volume. The segmentation of 3D models exhibits diverse methodologies, such as Zhang's [7] approach, which employs the topology of the part derived from its skeleton. The partitioning process entails cutting the equivalent topological skeleton into line or curvature segments. Luo [9] introduces a framework for dividing large-scale models into printable volumes, considering printability, connector feasibility, and assembleability, with an emphasis on minimizing the overall number of sub-volumes. Jadoon's [11] method, based on user interaction and a constrained tree algorithm, aligns with similar objectives. Wang [12], with a focus on enhancing surface finish, presents a decomposition method where each segment optimally addresses surface finish concerns under its unique building direction. Chen [13] introduces a novel stacking-based decomposition method for building up geometry through the aggregation of sub-volumes. Feature-based decomposition strategies, such as Lee's [14] partitioning of geometries with overhanging surfaces into prismatic shapes, and Wu's [15] beam-guided search for clipping planes, serve specific goals. Hergolz's [12] approach involves a search along the Z direction for manufacturable volumes, while Gao's [16] genetic algorithm-based decomposition method aims to minimize the number of cuts. Human-involvement is necessitated in Gao's method, where the specification of cutting planes and the computation of such planes entail a time-intensive process. Doherty [17] introduces a scheme

involving decomposing 3D models into feature-based geometries via STL representation, emphasizing joint stiffening between features. The aforementioned decomposition strategies predominantly yield planar cuts, facilitating fabrication on 2D surfaces. In contrast, Ding [18] introduces a process planning system for robotic AM systems, integrating decomposition based on overhang surfaces and multi-axis slicing techniques. Zhao [19] proposes feature-based decomposition based on concave edges, applicable to models with closed-concave edge loops. Ding [20] extends concave edge decomposition to mesh geometries for multi-directional deposition, with a limitation on geometries where two or more features converge at the same point. More recently, Nguyen [21] introduces a CAD model decomposition method using centroidal axes, applicable specifically to tree-shaped geometries.

In the pursuit of fully harnessing multi-axis capabilities, certain research endeavors have proposed fabrication strategies (see Fig. 3) involving continuous material deposition across multiple axes, coupled with repositioning of the building geometry [10, 22–24]. The three existing multi-axis deposition strategies can be summarized as follows:

a) adaptive slicing: computation of "buildable volumes" through a sequence of planar sections (Fig. 3a)
b) voxel deposition: determination of "upon voxels" via an optimized pathfinding algorithm within the entire volume (Fig. 3b)
c) geodesic iso-curve contours: calculation at a surface point x involving geodesic circles centered at x for a range of specified geodesic radii (Fig. 3c)

Figure 3 illustrates that these three representative M-AM deposition strategies exhibit distinct differences, each with its own limitations:

i. *Adaptive slicing*: Adaptive slicing methodologies dynamically adjust layer thickness based on local geometric features, enabling finer resolution in high-detail areas while maintaining efficiency in less complex regions. However, current adaptive slicing strategies in M-AM primarily focus on toolpath generation for single-body volumes, neglecting multi-feature interactions, convexity constraints, and global collision considerations. Existing algorithms often assume a single contiguous geometry, failing to account for multiple interconnected or disjoint features, which can result in discontinuities in deposition paths, particularly when transitioning between adjacent features with differing local layer thicknesses. Moreover, traditional adaptive slicing applies planar slicing operations without considering the convexity of the underlying geometry, leading to suboptimal segmentation and unsupported overhanging regions. Sharp transitions between adjacent slices further increase the risk of geometric distortions during fabrication. Additionally, current implementations lack integrated global collision avoidance mechanisms, assuming that layer-wise movements are inherently non-interfering. In multi-axis deposition systems, this omission can lead to unexpected tool collisions with previously deposited material or auxiliary structures, particularly in intricate or inward-facing geometries, ultimately compromising process reliability and part quality [25].
ii. *Voxel deposition*: Voxel-based deposition techniques discretize the build volume into a grid of uniform or adaptive-resolution volumetric elements (voxels), enabling a layer-wise material placement strategy. Despite advantages in geometric representation and simulation-based analysis, voxel-based deposition presents challenges related to deposition fidelity, geometric approximation, material transitions, and structural stability. Voxelized representations inherently introduce sampling artifacts, where insufficient resolution can lead to missing or skipped depositions, particularly in thin-walled regions where voxel centers fail to align precisely with target geometries. Geometric approximation errors arise due to the stair-stepped nature of voxel discretization, reducing surface smoothness and requiring significantly higher computational resources to improve resolution. Additionally, in multi-material or gradient material deposition, voxel-based tech-

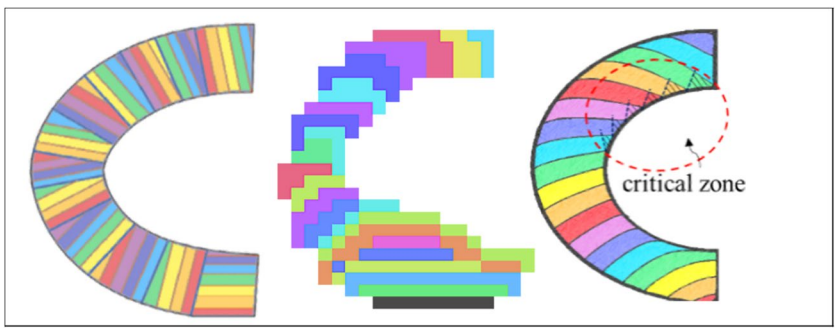

Fig. 3 An example illustrating current and proposed toolpath on a "C-shape," colors are used to indicate different layers: **a** adaptive slicing, **b** voxel deposition, and **c** geodesic iso-curve contours

niques struggle with boundary precision, as voxel discretization does not inherently account for material diffusion effects or thermal interactions, leading to weakened interfacial bonding in functionally graded structures. Deposition stability is further compromised by localized void formation, where discrete material placement introduces stress concentration points, negatively impacting mechanical properties. Unlike continuous toolpath-driven approaches, voxelized builds exhibit anisotropic mechanical behavior, particularly if voxel-to-voxel bonding is not sufficiently optimized during the fusion process, ultimately limiting their applicability in high-precision M-AM applications [26].

iii. *Geodesic iso-curve contours*: Geodesic iso-curve contours are based on the computation of lengths $l_x(r_i)$ of isocontours around a surface point x on the model. These contours will be used to define the boundaries of the freeform layers. However, they are not optimized for M-AM manufacturability, resulting in certain layers that are neither support-free nor self-supporting. Additionally, they do not account for local and global collisions. These layers tend to be freeform, often with unnecessary changes in building orientation, which increases the overall build time. Consequently, challenges arise in fully covering the underlying layer, leading to localized overhanging volumes. Addressing these issues requires meticulous management of deposition materials, including strategies such as dynamic reorientation of the geometry and adjustment of process parameters to effectively handle the complexities of these critical regions [10, 22].

Compared to conventional 3D printing, the 3D curved layer creation for filling up the geometry tremendously increases the computational complexity. Furthermore, two additional degree-of-freedom adduces the curved layers that make it challenging in determining the geometries that can be built based on the curved layer. The 3D freeform layers cannot be arbitrarily defined; otherwise, the combination of the 3D layers cannot form the original geometry or the collision between the deposition nozzle and the existing geometry will occur. In addition, preventing collision trajectory should be taken into consideration when sequencing 3D freeform layers where each depositing path needs to sit on top of the other volume. A feasible solution needs to consider input geometry as well as the M-AM machine manufacturing constraints. Major solutions are using convex/concave decomposition [27–29] methods to segment the given CAD model into sub-volumes, and then the planar toolpath can be arranged to be filling up the geometry. These methods usually cause collision between the nozzle and the printing head. Moreover, the addition of all decomposed volumes is not equal with the original geometry.

In this paper, we introduce an advanced toolpath generation algorithm aimed at supplanting the prevailing planar or decomposition approach utilized in the M-AM process. Our methodology leverages the manufacturability of M-AM systems to compute printable layers. The proposed algorithm operates by treating the upon surfaces of the as-built structure as viable supportive surfaces for the adjacent layer. It then computes the 3D printable layers by analyzing unsupported volumetric data with the M-AM machine constraints, ensuring collision-free interactions with the self-support system.

The problem can be articulated as follows: Given a 3D solid model M, we aim at finding a sequenced series of 3D curved "printable" layers $\{layer_i\}_{i=1,\ldots,n}$, which can be accumulated to form the solid model M. It is crucial to note that the "printable" layer does not denote a physical printed volume within the geometry; rather, it denotes a hypothetical surface that could be either self-supported or supported by preceding layers. The principal aim is to ensure that layer's manifest either planar or freeform attributes and can function as supportive volumes for the successive layer, capitalizing on the multi-axis rotatabilities inherent in the system. Termed as 3D "printable" layers are required to adhere to the following condition:

1. The $layer_{i+1}$ can be fully deposited/mapped on top surface of the $layer_i$
2. The $layer_i$ can be printed within the availability range of machine rotating angle

Consider $layer_i$ and $layer_{i-1}$ are adjacent printable layers with parametrization:

- $layer_i = r_i(u, v)$, where $(u, v) \subset \mathcal{R}^2$
- $layer_{i-1} = r_{i-1}(s, t)$, where $(s, t) \subset \mathcal{R}^2$

The normal vector to the $layer_i$ at a random point $r_i(u, v)$ is given by: $n_i(u, v) = \frac{\partial r_i}{\partial u} \times \frac{\partial r_i}{\partial v}$.

For every point $r_i(u, v)$ on $layer_i$, the condition that needs to be met is:

$r_{i-1}(s(u, v), t(u, v)) = r_i(u, v) + \lambda(u, v)\bullet - n_i(u, v)$, where λ is a scalar factor.

To conduct the M-AM in a continuous process, the input M needs to be computed into N consecutive "printable" layers, where:

- $M = \bigcup_i (layer_i) \,||\, layer_i \bigcap layer_j = \varnothing, with i, j represent random layers in the sequence$
- $n_i \cap \left(\cup_i \left(layer_i\right)\right) = \varnothing$, ensuring no interference of the collision when there exists multi-body within one layer

Two specific contributions addressed are:

- An algorithm based on the volumetric computation of the feasible printing volume based on the existing shape in the M- AM process.
- 3D curved toolpath generation from the 3D "printable" layer, that first slice the volume into 3D curved layers with feasible printing height, and then filling the layer with curved toolpath.

The proposed approach facilitates the processing of various models necessitating support structures in traditional 3D AM processes. It calculates the sequential 3D "printable" layers and toolpaths without the need for support structures, leveraging the ability to continuously orient the building geometry during material deposition.

2 Methodology

The delineation of the "printable" layer is contingent upon its capacity to be constructed autonomously without the requirement of support structures; a prerequisite dictated by stringent manufacturability considerations. This entails adherence to a set of rigorous criteria and specifications to ensure the feasibility of generating the layer within the parameters of the M-AM scheme.

The fundamental definition of a "printable" layer necessitates meticulous attention to structural and geometrical constraints. The layer must exhibit inherent self-supporting characteristics, obviating the need for supplementary support structures during its fabrication. This demand for autonomous construction without external supports is anchored in the overarching goal of enhancing the efficiency and cost-effectiveness of the additive manufacturing workflow. The manufacturability criteria encompass various facets, including geometric complexity, overhang angles, and material behavior during deposition. The printable layer is intricately designed to navigate these challenges without compromising structural integrity or dimensional accuracy. The objective is to create a layer that seamlessly integrates into the overall build, ensuring a smooth and uninterrupted M-AM process.

In essence, the definition of a printable layer, as elucidated herein, serves as a pivotal parameter in the optimization of additive manufacturing processes, strategically aligning with the overarching goal of achieving support-free manufacturability while maintaining precision and structural robustness.

Criterion I: $layer_i(\text{unsupported}) = layer_i \cap \sum_{i=1}^{n} \sum_{p \in S_i} V(p)$

Define $S_i \subset L_i$ as the set of unmapped points in planar layer L_i along a predefined slicing orientation (see criterion IV). In here, a point $p \in L_i$ is considered unsupported if $p + \lambda(u, v) \bullet [0,0,-1] \cap L_{i-1} = \varnothing$

Criterion II: $\exists r(u_1, v_1)$ and $r(u_2, v_2)$ on $layer_i(\text{unsupported})$ $||\forall \alpha \in [0,1],\ \exists r_a = \alpha r(u_1, v_1) + (1-\alpha) r(u_2, v_2)$ on $layer_i$ (unsupported).

The convexity of the unsupported area through initial direction e.g., [0,0,1] on printable layer can be maintained, to avoid local collision, see Fig. 4 below.

Criterion III: $\forall p \in layer_i,\ R(p + v \bullet n_p) \cap layer_i = \varnothing || R(p + v \bullet n_p) \cap Substrate, Table = \varnothing$

This ensures no local collision and global collision from the titled nozzle, in here, v is the length of nozzle; $R(p + v \bullet n_{pi})$ is a cylinder representation with nozzle radius R at any point on a printable layer with a defined nozzle length.

Criterion IV: $\forall layer_i,\ \exists n_{layeri} = [x_{layeri}, y_{layeri}, z_{layeri}]$, $\nexists (contour(C_{layeri}) - contour(C_{layeri-1})) \cap contour(C_{layeri-1}) = \varnothing$. $\{C_{layeri}\}$ are planar slicing layers of $M - \cup layer_i$ with n_{layeri}.

This approach ensures there are no unsupported volumes in the remaining layers along the specified direction. Here, we predefine a direction for any printable layer. When performing normal planar slicing on the unsliced portion of the model along this direction, if a layer is found to have more contours than the previous layer, and more than one of these contours lacks an overlapping zone with the previous layer,

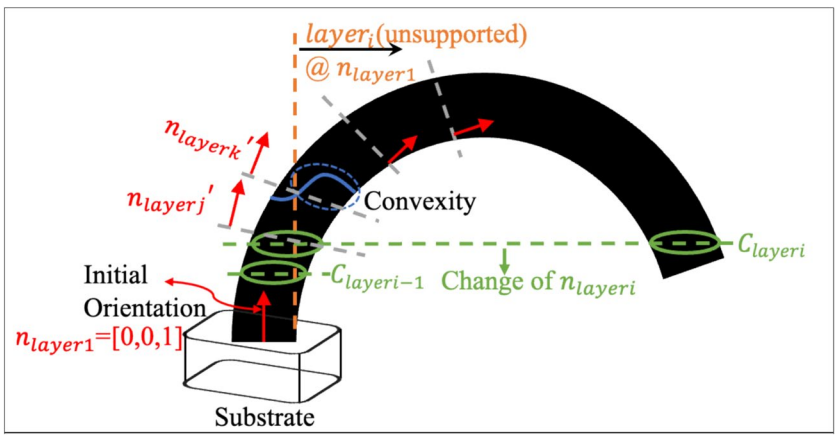

Fig. 4 Exemplary explanation of abovementioned criteria

it indicates a need to switch the predefined direction. Refer to the exemplary Fig. 4 below for illustration.

Criterion V: $\forall layer_i$, $\exists n_{layer} = [x_{layer}, y_{layer}, z_{layer}]$, $\exists (contour(C_{layeri}) - contour(C_{layeri-1})) \cap contour(C_{layeri-1}) = \varnothing$, $n_{layeri}\prime = n_{layeri}\cos(\theta) + (u \times n)sin\theta + u(u \bullet n)(1 - cos\theta)$, subject to min $\left\|u - n_{layer}\prime\right\|^2$, till $\nexists (contour(C_{layeri}) - contour(C_{layeri-1})) \cap contour(C_{layeri-1}) = \varnothing$. u is the rotation axis with $|u|=1$. $\{C_{layeri}\prime\}$ are planar slicing layers of $M - \cup layer_i$ with $n_{layer}\prime$.

If Criterion IV is not met, it is necessary to reorient the predefined direction for the printable layer. This criterion seeks a new direction that requires minimal rotation while ensuring no unsupported volumes remain for subsequent layers. Refer to the exemplary Fig. 4.

Criterion VI: min $\sum_{i=1}^{N} \left|\left|n_i - n_{layeri}\right|\right|^2$, with $p \in layer_i$ and its normal n_{pi}.

This implies minimizing the variance of the printable surface normals to efficiently reduce the required rotational motion. $\forall p \in layer_i$, with each n_{pi} should remain normalized, i.e., $\|n_{pi}\|=1$, $n_{layeri} \neq \frac{1}{N}\sum_{i=1}^{N} n_i$.

To satisfy the specified criteria, the following algorithm represents a sophisticated and efficient methodology for the systematic generation of a series of 3D printable layers. This algorithm is designed to leverage topological information and manufacturability constraints, ensuring the synthesis of a geometric space that adheres to the abovementioned criteria while efficiently reducing the amount of rotational motion on the M-AM process. By rigorously analyzing the topological characteristics of the geometry, the algorithm identifies unsupported areas and constructs a printable layer with boundary representation that facilitates self-supporting features, thereby reducing the need for auxiliary supports during the AM process. Concurrently, manufacturability considerations are seamlessly integrated into the construction criteria. This proposed algorithm strategically balances geometric complexity and fabrication feasibility, resulting in an optimized layering strategy for M-AM without compromising structural integrity.

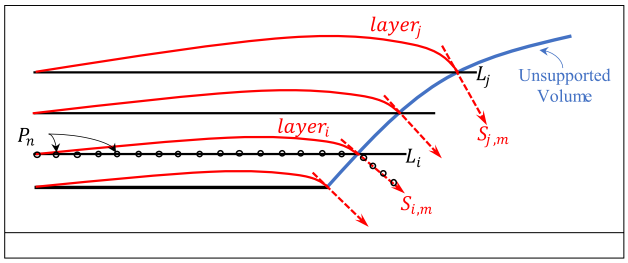

Fig. 5 Visualization of the creation of printable layer—$layer_i$

Algorithm 1: Generation of 3D printable layers

Input: CAD Model *M*(such as: .stp,.stl ...), initial building orientation, e.g., $o_1(0,0,1)$

Output: Continuous 3D printable layers $\{layer_i\}$

$\cup \{L_i\} = slice(M)$, along with n_{layeri}
$e_{i,m} = L_i \cap M$
$S_{i,m} = \perp M|e_{i,m}$
if $\measuredangle(S_{i,m}, o_1) > \frac{\pi}{2}$
  $edge_{i,type1} = \cup (e_{i,m})$
else
  skip
end
$d_i = e_{i,m} \cup S_{i,m|edge\ i,type1}$
Define $\{P_1, P_2, \ldots, P_n\}$ on d_i, $\ni d_i(t)=(1-t)\ P_n + tP_{n+1}$, $t \in [0,1]$
Define printable layer i as $\boldsymbol{layer_i} = S(u,v)$, $\ni S(u,v) = (x(u,v), y(u,v), z(u,v))$
Min$(\sum_{i=1}^{n}||P_n - S(u_n, v_n)||^2)$, $||.||$ denotes the Euclidean distance, and (u_n, v_n) are the parameters corresponding to each P_n

This algorithm is designed to systematically categorize edges within a given structure, with a particular emphasis on efficiently computing a self-supported surface topology on the identified overhanging volumes. The algorithm employs a norm calculation to determine the angle between an edge's normal vector and the build orientation. Edges with a normal vector forming an angle exceeding 90° relative to the build orientation are marked for further analysis. These edges will be constructed with tangent surfaces concerning the adjacent surfaces on the model. The categorized edges, along with their contours on the tangent surfaces, and the remaining edges associated with the parameter L_i, will undergo a random point generation process. These points will define a freeform printable layer where criterion V is met. The generation of these points follows a specified randomization process, and their spatial distribution is crucial for creating a freeform layer that adheres to the underlying geometry. During the creation of the freeform layer topology, a minimum least squares fit methodology is employed. This approach ensures that the randomized points align optimally with the underlying geometry, minimizing overall deviation from the intended freeform design. Figure 5 presents a visual representation of the algorithm.

As shown in Fig. 5, $layer_{i+1}$ is a freeform surface that is constructed under the following conditions: (i) available self-supported volume that is calculated from $layer_i$, (ii) formation by the unsupported volume constraints from remaining body ($M - layer_i$). The algorithm undertakes a volumetric analysis to determine the spatial extent defined by surface constraints within the extant geometry. In detail, the algorithm evaluates the volume enclosed by predefined surface constraints, ensuring the resulting geometry meets the necessary conditions for seamlessly integrating overhanging volumes. The primary aim is to confirm that the geometry facilitates the systematic layering of surfaces, particularly in establishing perpendicular relationships between the overhang surface and the preceding layer. This volumetric assessment acts as a crucial preliminary step in the construction process, offering a quantitative measure of available space and compliance with geometric constraints. Consequently, the algorithm lays a robust groundwork for subsequent fabrication stages, enhancing the precision and efficiency of the overall construction process by methodically addressing spatial requirements dictated by the specified surface constraints.

M-AM provides the capability of re-orienting the building geometry while the material is depositing which further allows continuously re-orientating during the build. We define the volumetric representation of printable layer—working zone (w_i) based on $layer_i$ follows: $w_i = Volume(layer_{i-1}, layer_i)$. However, w_i does not maintain a constant thickness across $layer_i$, posing challenges for direct fabrication via commercial M-AM processes. This inconsistency would necessitate continuous adjustment of process parameters. Given a "*printable*" zone, $layer_i$ and a 3D volumetric working zone (w_i), our goal is to slice it into a set of 3D freeform sublayers—$\{sublayer_x\}_{x=1,\ldots,n}$ with equal material deposition height – uniform layer thickness, such that:

$$w_i = U_x\left(w\left(sublayer_x\right)\right), where, w\left(sublayer_x\right) \bigcap \mathrm{w}\left(sublayer_{x+1}\right) = sublayer_x \tag{1}$$

$$sublayer_x \left|\right| sublayer_{x+1} \left|\right| layer_i \tag{2}$$

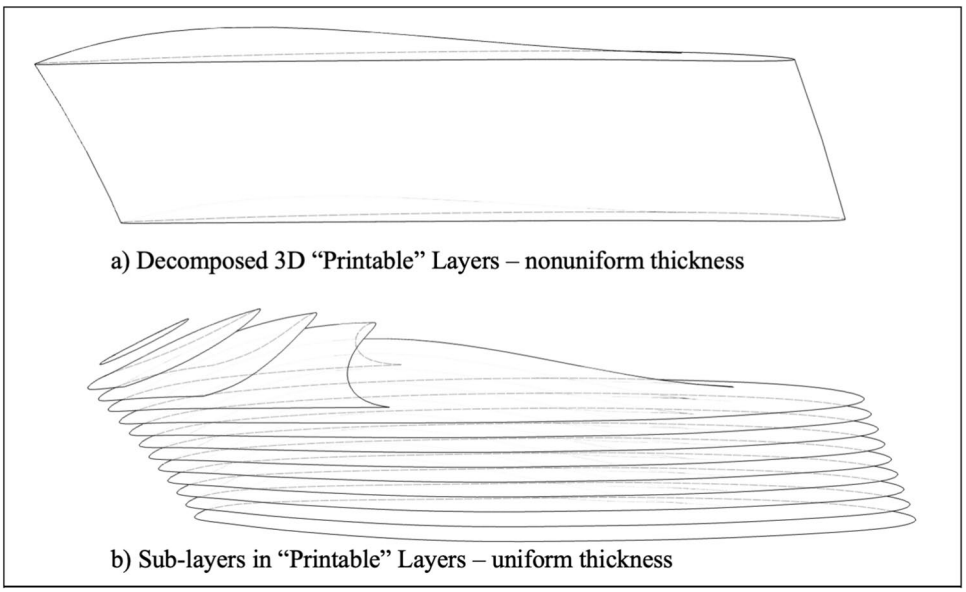

Fig. 6 Sublayers in one 3D "printable" layer

The algorithm initiates the extraction of a 3D "printable" layer, as delineated in Fig. 6a, wherein subsequent computations are executed to derive sublayers and their corresponding toolpaths. The segmentation process of the printable layer is governed by the layer thickness parameters inherent to the M-AM system, as depicted in Fig. 6. Figure 6b provides a visual representation of the sublayers within the identified "printable" layer, each sublayer delineated according to the specified layer thickness criteria dictated by the M-AM system. This segmentation is ensuring the precision and conformity of the resultant sublayers within the overall printing process.

The computational methodology employed to ascertain these sublayers entails a systematic assessment of the printable layer against the specified criteria. As illustrated in Fig. 5b, the resulting slicing ensures a uniform layer height across the sub-layers. Each distinct "printable" layer within the manufacturing process is intentionally configured to exhibit convexity, thereby imparting convex characteristics to its sublayers to prevent local collisions during processing. Specifically, the algorithm ensures unimpeded navigation for the deposition head across these sublayer surfaces, mitigating concerns regarding collisions with previously deposited layers or the layer currently being deposited. The further toolpath generation on these sublayers will complete the process planning configuration which involves a conversion from the three-dimensional (3D) space to a series of deposition surfaces, constituting a 3D to 2D conversion process. Subsequently, these 2D deposition surfaces are subjected to the calculation of freeform toolpaths, representing a further translation from the two-dimensional (2D) representation to a one-dimensional (1D) linear toolpath. Each sublayer can be defined by parametric equations $sublayer(u, v)$, where u and v are the parameters that describe points on the surface. The toolpath generation follows:

- Define a set of parameter values u_i and v_j within the allowable range for the surface.
- Evaluate the surface equation at each combination of u_i and v_j to obtain the corresponding points $S(u_i,v_j)$
- Connect adjacent points with equal u values to form isoparametric curves in the u-direction.
- Connect adjacent points with equal v values to form isoparametric curves in the v-direction.

Figure 6 illustrates the process of processing sublayers by adjusting the orientation of the nozzle to adhere to the self-supported rule, ensuring that the nozzle remains perpendicular to the surface. This progression, from designing convexity to generating sublayers, converting them into deposition surfaces, and finally extracting toolpaths along isoparametric curves on these sublayers, constitutes a multi-step procedure crucial for the precision and efficiency of the M-AM workflow. Figure 7 depicts the 3D sublayer along with the toolpath and the cumulative toolpath on its related printable layer.

The computation of the toolpath for individual sublayer necessitates the precise determination of both the position and orientation of the material deposition head. In our machine setup (5axisMaker), the M-AM system adopts a

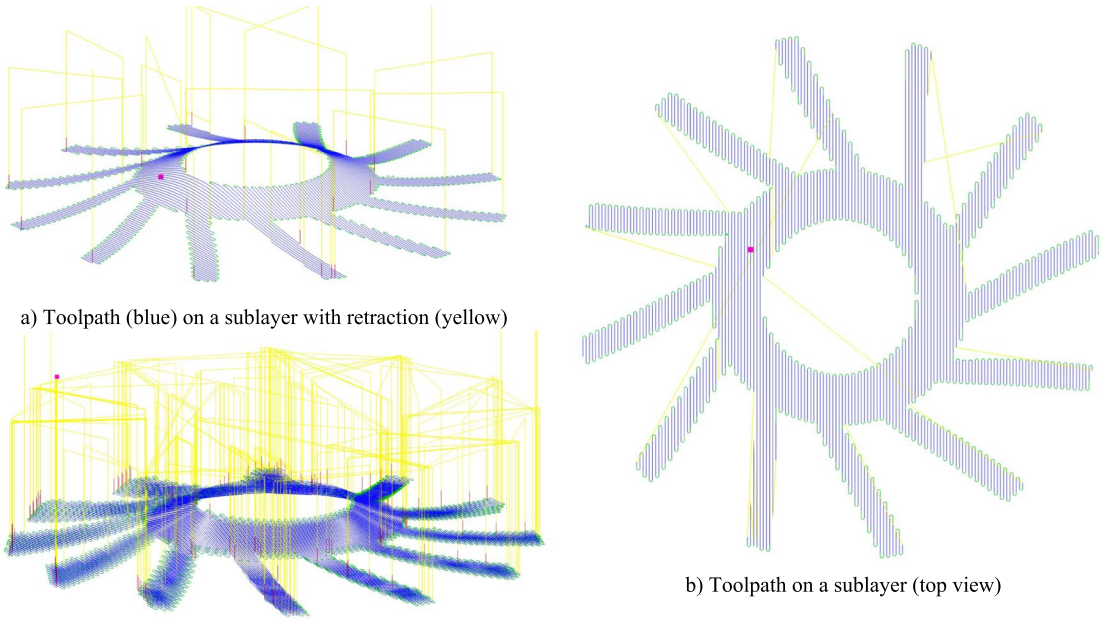

a) Toolpath (blue) on a sublayer with retraction (yellow)

b) Toolpath on a sublayer (top view)

c) Cumulative toolpath on a printable layer

Fig. 7 Layered toolpaths on one sublayer and printable layer on a turbine

5-axis configuration, featuring B and C rotary functionalities on the deposition nozzle. By integrating topological information specific to each sublayer and factoring in the positioning and orientation requirements of the tool path, the inverse kinematics can precisely calculate the motion necessary for the rotary axes to accomplish the desired material deposition orientation. This integration facilitates the optimal utilization of the system's 5-axis capabilities, thereby enhancing the efficiency and efficacy of the manufacturing process.

3 Result and discussion

The algorithm is implemented within the Rhino Grasshopper environment. To demonstrate the practical efficacy of the implemented algorithms, various example parts were subjected to processing within the developed software framework. These sample parts, drawn from the corpus of existing literature, serve as illustrative instances wherein the algorithms orchestrate the formation of layers and subsequent toolpath generation.

Figure 8 presents a visual representation of the two sample processed models, each illustrating the layered construction and associated toolpaths generated by the implemented software. It is important to highlight that these models, although grounded in existing literature, either depict scenarios requiring algorithmic intervention for volumetric decomposition or cannot be processed in a self-supported manner without encountering collisions (e.g., the arch example). The fundamental challenge lies in extracting suitable volumes, which either necessitates adapting existing toolpath strategies or presents difficulties in achieving a feasible multi-axis deposition solution. The algorithmic proficiency demonstrated in these examples underscores the algorithm's capability in addressing complex geometric scenarios, thereby contributing to the advancement of M-AM methodologies in situations where

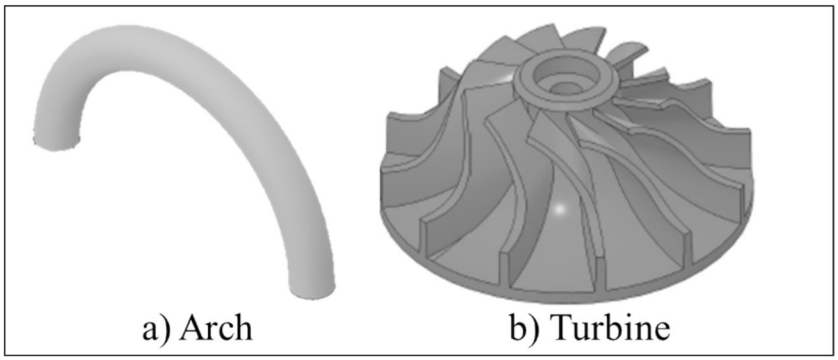

Fig. 8 Input models for proposed M-AM strategy

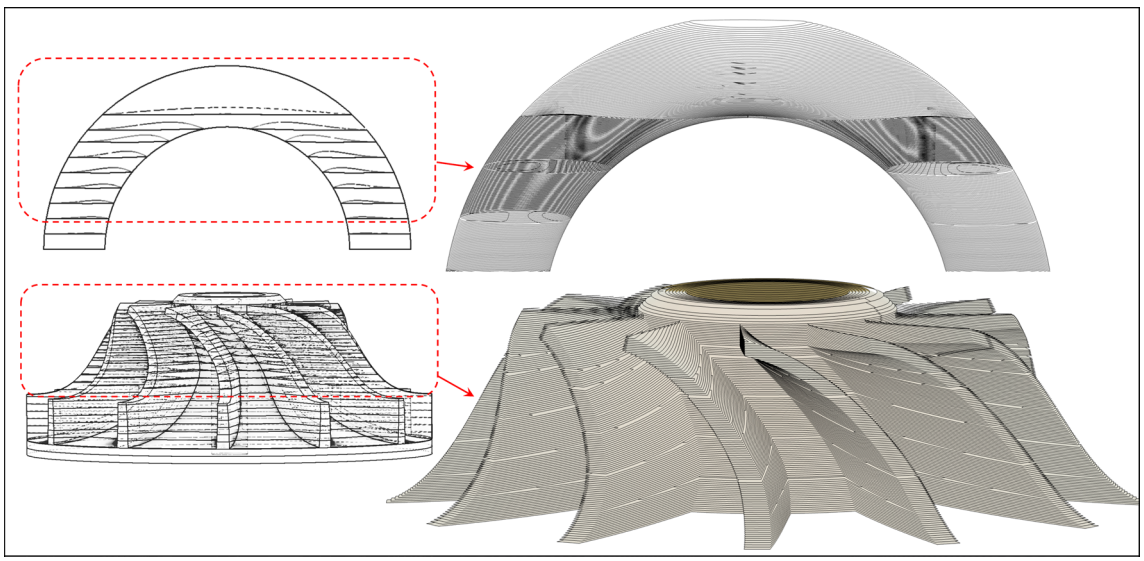

Fig. 9 "Printable" layer visualization of two sample models

manual decomposition or traditional strategies prove inadequate.

The visual depiction of the "printable" layers is presented in Fig. 9 left, offering a demonstrative illustration of the effectiveness of the proposed M-AM freeform deposition approach. These layers, generated through the outlined algorithm, exemplify the strategic coordination of material deposition. The overall sublayers are shown in Fig. 9 right. Each layer showcases the meticulous control exerted over the multi-axis deposition system, enabling precise navigation of intricate geometries and the fabrication of complex structures with finesse.

The freeform "printable" layers depicted in Fig. 9 provide valuable insights into the algorithm's ability to address the complexities inherent in certain "impossible" geometries, particularly in leveraging unsupported volumes to create self-supported printable layer surface topologies. In the conventional planar 3D printing process, the merging points, as depicted in Fig. 9(a) and (c), denote instances where two distinct bodies or components from at least two or more printed features converge into a single body during the printing process. The convergence points pose a challenge, requiring the addition of support structures to prevent printing defects like "telephone wires" or areas with compromised structural integrity. To tackle this challenge, the proposed M-AM strategy adopts a unique slicing method, segmenting the object into curved layers. This slicing approach ensures that each printable volume of the object is supported by the preceding volume, minimizing the requirement for extensive support structures and averting collisions.

After identifying the printable layers, subsequent sliced sublayers within each printable layer are generated. The goal was to ensure that each sublayer has a feasible printing height that adheres to the practical constraints and capabilities of the M-AM system. To validate the effectiveness and feasibility of these constructed sublayers, a testing phase was conducted using the 5axisworks platform—a multi-axis fused deposition modeling (FDM) process on a 5axisMaker printer. Figure 10b illustrates the detailed multi-axis material deposition process of the arch sample at various stages within the M-AM setup.

The experimental validation conducted on the 5axisworks platform provides a rigorous assessment of the practical feasibility, structural integrity, and deposition accuracy of the developed sublayers within a multi-axis fused deposition modeling (FDM) environment (Fig. 11). The 5-axis FDM process offers a deposition strategy that closely emulates the complexities of M-AM by enabling non-planar, multi-directional material extrusion, making it an ideal testbed for evaluating the manufacturability constraints and geometric adaptability of the generated sublayers. The visual representation of each stage in Fig. 9 b not only documents the testing procedure but also offers valuable insights into the interaction between the sublayers and the dynamic positioning mechanisms within the M-AM system.

To comprehensively assess the advantages of the proposed M-AM freeform deposition strategy, two comparative arch samples are fabricated under different conditions:

- Planar layers without support structures—a conventional 2.5D slicing approach, where each layer is deposited parallel to a fixed build plane without additional support, exposing overhanging regions to potential collapse or deformation.

Fig. 10 Arch with constructed freeform printable layers with the M-AM deposition process

Fig. 11 Turbine with constructed freeform printable layers with the M-AM deposition process

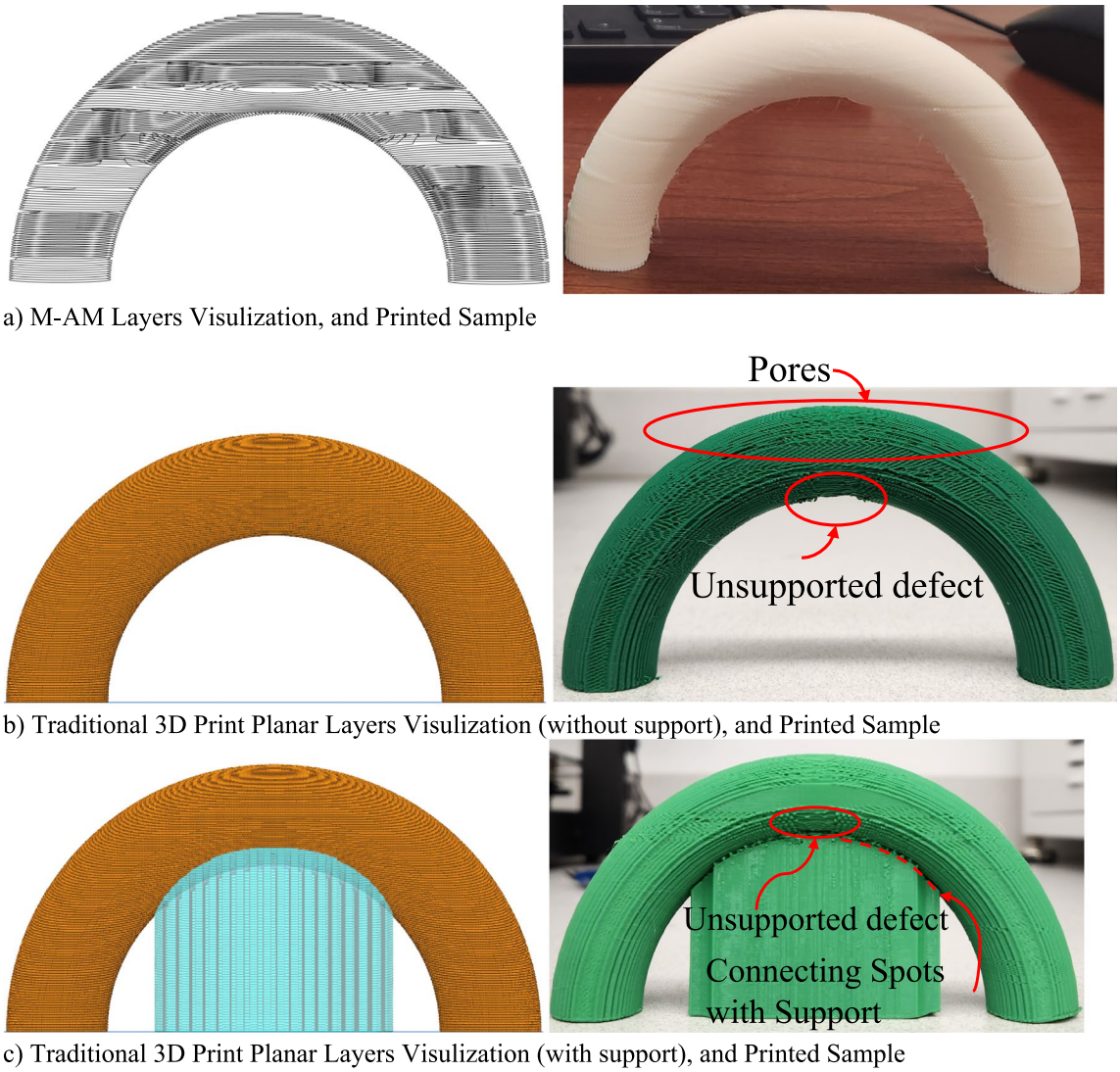

a) M-AM Layers Visulization, and Printed Sample

b) Traditional 3D Print Planar Layers Visulization (without support), and Printed Sample

c) Traditional 3D Print Planar Layers Visulization (with support), and Printed Sample

Fig. 12 Three arch samples based on three deposition strategy: freeform M-AM, planar without support structure, and planar with support structure

- Planar layers with support structures—a standard supported AM strategy, where auxiliary support materials are introduced beneath overhanging features to ensure structural stability, with the increased material consumption and post-processing requirements.

These arch samples are printed with same material = PLA, printing speed = 30 mm/s, layer thickness = 0.2 mm, hatch spacing = 0.2 mm, and toolpath pattern within a layer = linear with 90-degree rotation per layer. These printed arch samples are shown in Fig. 12.

Observing Fig. 12, it is evident that the arch sample fabricated utilizing the proposed M-AM strategy exhibits better surface finish, particularly on regions characterized by large curvature, in contrast to the other two samples manufactured using traditional planar layering techniques. Notably, samples produced via conventional 3D printing methods display noticeable defects on their surfaces, including porosity and "telephone-wired" anomalies attributed to unsupported volume during the printing process. These defects are visually apparent and are anticipated to detrimentally affect the structural integrity and mechanical properties of the printed parts.

These samples undergo compression testing to evaluate their structural performance. The notation used for classification is as follows: "*P*" represents an arch fabricated using a conventional 2.5D planar build; "*PS*" denotes an arch constructed with a 2.5D planar build incorporating support structures, and "*F*" designates an arch produced using the M-AM freeform deposition strategy. There are two compression tests conducted for these samples, which the experimental setup has shown in Fig. 13.

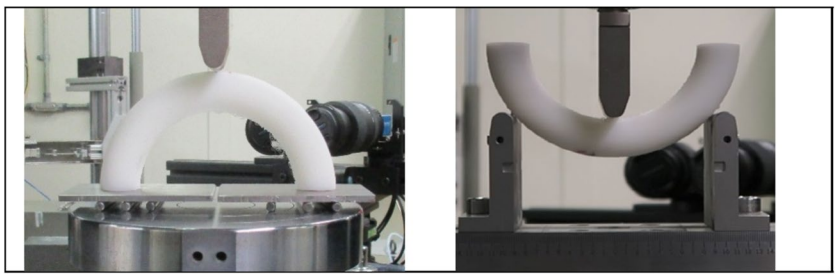

Fig. 13 "*n*" and "*u*" compression test setup for the arch samples

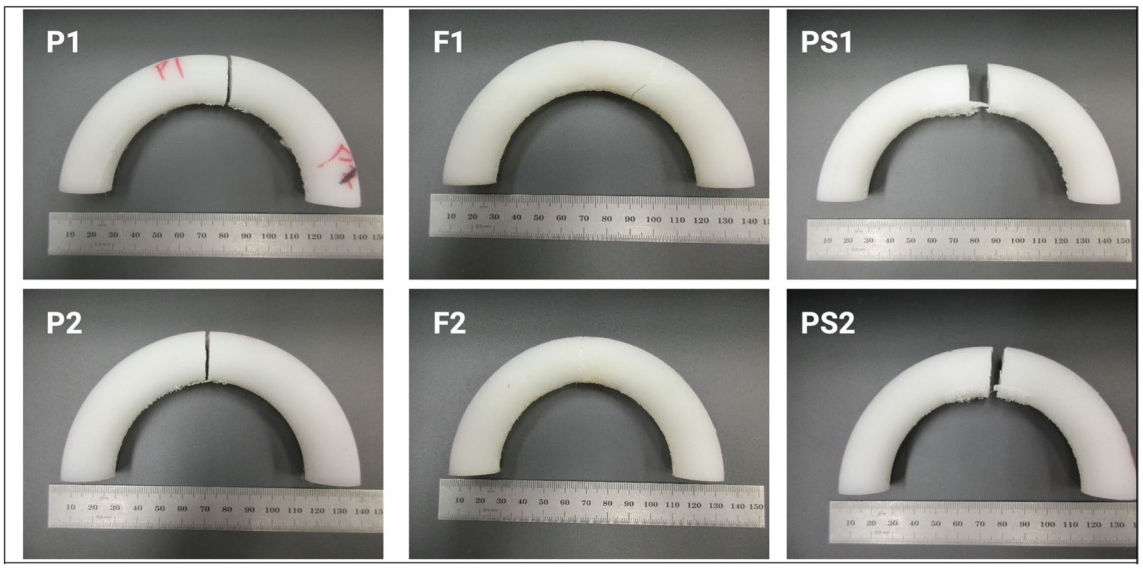

Fig. 14 Final arch after "*n*" and "*u*" compression tests

The test setup consists of a 100-mm supporting fixture span, ensuring uniform boundary constraints to accurately evaluate bending resistance. A pushing rate of 1 mm/min maintains a consistent displacement-controlled testing condition. This slow and controlled loading rate minimizes dynamic effects and allows for precise measurement of stress–strain behavior, yield point, and ultimate bending load. The test is designed to characterize the mechanical response of different deposition strategies, including elastic deformation, plastic yielding, and fracture initiation. The final fracture patterns and crack propagation are illustrated in Fig. 14, providing a detailed visual representation of failure modes across different samples.

The freeform layer alters stress distribution due to the non-linear orientation of the deposition layers, which contrasts with the uniform, orthogonal structure of planar-layered prints. In a freeform structure, the deposition follows more complex trajectories that are often aligned with the principal stress directions, enabling the material to more effectively distribute applied loads throughout the part. This approach reduces the occurrence of localized stress concentrations typically seen in planar-layered structures, where layers are deposited in a consistent, horizontal fashion. In planar-layered designs, stress tends to concentrate at the interfaces between layers due to the inherent weakness in the interlayer bond, making them susceptible to crack propagation or failure under load. By contrast, the freeform method allows for a more integrated and continuous stress path across layers, with the non-parallel arrangement of the deposition lines enhancing the material's ability to bear loads without abrupt changes in stress direction. This effectively mitigates weak spots where cracks may form, leading to a more uniform distribution of stress. Figure 15 presents the load–deflection curves under "*n*" and "*u*" compression tests.

From the experimental results, it is evident that the specimens fabricated using the freeform layering strategy exhibit significantly higher stiffness compared to those constructed with planar layering. This non-uniform orientation enhances the material's ability to transfer loads more efficiently across the structure. The result is a structure that exhibits higher stiffness and greater resistance to deformation under loading conditions, with better overall performance in sustaining mechanical stresses.

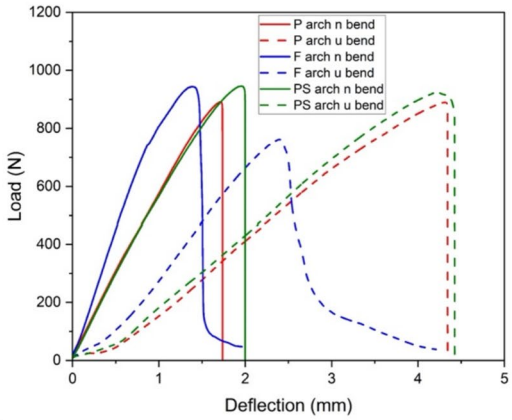

Specimen (Bend style)	Min. Diameter, in	Outer span, in	Failure in bend test
P1 (n)	0.798	4.739	Brittle fracture
P2 (u)	0.796	4.7315	Brittle fracture
F1 (n)	0.7545	4.705	Cracked
F2 (u)	0.765	4.7045	Cracked
PS1 (n)	0.8015	4.75	Brittle fracture
PS2 (u)	0.807	4.7225	Brittle fracture

Fig. 15 Load–deflection curve for all arch samples under "*n*" and "*u*" compression tests

4 Conclusion and future work

A novel deposition strategy is introduced herein, leveraging the capabilities of M-AM techniques to depart from the conventional layer-by-layer material deposition paradigm. This strategy involves a continuous printing process across varied building orientations, eliminating the need for support structures. Notably, the prevailing methods for fabricating geometries using M-AM processes typically mandate a prerequisite decomposition of the model into single-body volumes. In existing techniques, the computation of 3D layers for each individual single-body volume, coupled with the determination of the medial axis, is undertaken. However, challenges persist, for example, there will exist "weld lines" between each decomposed volume. In addition, in addressing bridging geometries, which currently remains unresolved for continuous layers without collision, this necessitates the decomposition of the model, limiting the efficiency of the fabrication process.

In response to these challenges, we propose an innovative technique for calculating the "printable" volume, enabling the accumulation of material based on the existing printed geometry. The "printable" layers, structured as convex shapes, guarantee the accessibility of the deposition nozzle while maintaining a collision-free deposition environment. Our algorithm initiates by generating volumes that can be successfully constructed based on the previous layer, achieved through the creation of self-supported surface feature based on unsupported volumes. Subsequently, sequenced sublayers within each "printable" layer, contingent on the M-AM process feasible layer thickness, are extracted, and linear toolpaths for covering these sublayers are computed.

The proposed algorithm can successfully compute the direct freeform printing toolpaths for complicated models featuring large overhangs. Ongoing efforts are directed towards enhancing algorithmic performance, focusing on accelerating computational speed. Moreover, experimental analyses will be conducted with relevance to the structural integrity through this novel M-AM fabrication strategy, with the ultimate goal of transforming M-AM into a less human-involved but more consistent and high-end quality manufacturing process.

Acknowledgements We acknowledge Dr. Wei Tang at ORNL for his assistance in conducting the compression analysis.

Funding This work is financially supported by Oak Ridge National Lab under the contract CW52925/4000216485.

Declarations

Conflict of interest The authors declare no competing interests.

References

1. Wohlers T, Gornet T, Mostow N, Campbell I, Diegel O, Kowen J, ..., Peels J (2016) History of additive manufacturing
2. Allaire G, Dapogny C, Estevez R, Faure A, Michailidis G (2017) Structural optimization under overhang constraints imposed by additive manufacturing technologies. J Comput Phys 351:295–328
3. Delfs P, Tows M, Schmid HJ (2016) Optimized build orientation of additive manufactured parts for improved surface quality and build time. Addit Manuf 12:314–320
4. Xiao X, Joshi S (2020) Process planning for five-axis support free additive manufacturing. Addit Manuf 36:101569
5. Xiao X, Joshi S (2020) Decomposition and sequencing for a 5-axis hybrid manufacturing process. International manufacturing science and engineering conference (Vol. 84256, p. V001T01A049). American Society of Mechanical Engineers. https://doi.org/10.1115/MSEC2020-8385

6. Xiao X, Xiao H (2021) Autonomous robotic feature-based free-form fabrication approach. Materials 15(1):247
7. Zhang J et al (2000) Laser additive manufacturing process planning and automation. In: Proceedings of the 10th Annual Solid Freeform Fabrication Symposium, University of Texas Press 2000, pp 243–250
8. Feldhausen T, Heinrich L, Saleeby K, Burl A, Post B, MacDonald E, ..., Love L (2022) Review of computer-aided manufacturing (CAM) strategies for hybrid directed energy deposition. Addit Manuf 56:102900. https://doi.org/10.1016/j.addma.2022.102900
9. Luo L, Baran I, Rusinkiewicz S, Matusik W (2012) Chopper: partitioning models into 3D-printable parts. ACM Trans Graph 31(6):129:1–129:9. https://doi.org/10.1145/2366145.2366148
10. Dai C, Wang CC, Wu C, Lefebvre S, Fang G, Liu YJ (2018) Support-free volume printing by multi-axis motion. ACM Transactions on Graphics (TOG) 37(4):134
11. Jadoon AK, Wu C, Liu YJ, He Y, Wang CC (2018) Interactive partitioning of 3D models into printable parts. IEEE Comput Graphics Appl 38(4):38–53
12. Herholz P, Matusik W, Alexa M (2015) Approximating free-form geometry with height fields for manufacturing. Comput Graph Forum 34:239–251. https://doi.org/10.1111/cgf.12556
13. Chen X, Zhang H, Lin J, Hu R, Lu L, Huang QX, ... Chen B (2015) Dapper: decompose-and-pack for 3D printing. ACM Trans Graph 34(6):213–1
14. Lee K, Jee H (2015) Slicing algorithms for multi-axis 3-D metal printing of overhangs. J Mech Sci Technol 29:5139–5144
15. Wu C, Dai C, Fang G, Liu YJ, Wang CC (2019) General support-effective decomposition for multi-directional 3D printing. IEEE Trans Autom Sci Eng 17(2):599–610
16. Gao Y, Wu L, Yan DM, Nan L (2019) Near support-free multi-directional 3D printing via global-optimal decomposition. Graph Model 101034. https://doi.org/10.1016/j.gmod.2019.101034
17. Doherty S, De Backer W, Bergs AP, Harik R, van Tooren M, Rekleitis I (2016) Selective directional reinforcement of structures for multi-axis additive manufacturing. CAMX Compos Adva Mater Expo
18. Ding D, Pan Z, Cuiuri D, Li H (2015) Process planning for robotic wire and arc additive manufacturing. In 2015 IEEE 10th conference on industrial electronics and applications (ICIEA). IEEE 2000–2003. https://doi.org/10.1109/ICIEA.2015.7334441
19. Zhao G, Ma G, Xiao W, Tian Y (2019) Feature-based five-axis path planning method for robotic additive manufacturing. Proceedings of the institution of mechanical engineers, part B: Journal of Engineering Manufacture 233(5):1412–1424
20. Ding D, Pan Z, Cuiuri D, Li H, Larkin N, Van Duin S (2016) Automatic multi-direction slicing algorithms for wire based additive manufacturing. Robotics and Computer-Integrated Manufacturing 37:139–150
21. Nguyen L, Buhl J, Bambach M (2018) Decomposition algorithm for tool path planning for wire-arc additive manufacturing. J Mach Eng 18(1):95–106
22. Xu K, Li Y, Chen L, Tang K (2019) Curved layer based process planning for multi-axis volume printing of freeform parts. Comput Aided Des 114:51–63
23. Chen Y, Zhou C, Lao J (2011) A layerless additive manufacturing process based on CNC accumulation. Rapid Prototyping Journal 17(3):218–227
24. Pan Y, Zhou C, Chen Y, Partanen J (2014) Multitool and multi-axis computer numerically controlled accumulation for fabricating conformal features on curved surfaces. J Manuf Sci Eng 136:031007.
25. Huang Y, Zhang J, Hu X, Song G, Liu Z, Yu L, Liu L (2016) Framefab: robotic fabrication of frame shapes. ACM Transact Graph (TOG) 35(6):224
26. Zhao G, Ma G, Feng J, Xiao W (2018) Nonplanar slicing and path generation methods for robotic additive manufacturing. Int J Adv Manuf Technol 96(9–12):3149–3159
27. Demir İ, Aliaga DG, Benes B (2018) Near-convex decomposition and layering for efficient 3D printing. Addit Manuf 21:383–394
28. Hu R, Li H, Zhang H, Cohen-Or D (2014) Approximate pyramidal shape decomposition. ACM Trans Graph 33(6):213–221
29. Lien JM, Amato NM (2007) Approximate convex decomposition of polyhedra. Proceedings of the 2007 ACM symposium on solid and physical modeling. ACM 121–131. https://doi.org/10.1145/1236246.123626